Investigating Formate, Sulfate, and Halide Anions in Reversible Zinc Electrodeposition Dynamic Windows

Desmond C. Madu, Micah V. Lilo, Andrew A. Thompson, Hanqing Pan, Michael D. McGehee, and Christopher J. Barile^{1,*}

- 1. Department of Chemistry, University of Nevada, Reno, NV 89557
- 2. Department of Chemical and Biological Engineering, University of Colorado, Boulder, CO 80303, USA
- 3. Materials Science and Engineering, University of Colorado, Boulder, CO 80303, USA

^{*}E-mail: cbarile@unr.edu

Abstract

Reversible metal electrodeposition (RME) is an emerging and promising method for designing dynamic windows with electrically controllable transmission, excellent color neutrality, and wide dynamic range. Zn is a viable option for metal-based dynamic windows due to its fast switching kinetics and reversibility despite its very negative deposition voltage. In this manuscript, we study the effect of the supporting electrolyte anions for Zn electrodeposition on transparent tin-doped indium oxide. Through systematic additions or removal of components of the electrolytes, we are able to establish a link between the anions and the effectiveness of Zn RME. This insight allows us to design practical two-electrode 25 cm² Zn dynamic windows that switch to <1% within 20 s. Lastly, we demonstrate that the accumulation of Zn(OH)₂ species on the working electrode degrades the optical contrast of Zn windows during long-term cycling. However, the elimination of these species through acid immersion allows the windows to cycle at least 500 times. Reversible Zn electrodeposition in the presence of a polyethylene glycol additive further improves the cycle life to greater than 1,000 cycles. Taken together, these studies highlight important design principles for the construction of robust dynamic windows based on Zn RME.

Keywords: dynamic windows, reversible metal electrodeposition, zinc electrodeposition, indium tin oxide, electrolyte design

1. Introduction

Dynamic windows are electronically-controlled devices that change their transmission from a transparent state to an opaque state and vice versa.¹⁻⁷ These windows are a promising technology to reduce the amount of energy used in commercial and residential buildings with average energy savings of 10%.^{8,9} Buildings account for 40% of total energy used in the United States, and about half of that comes from heating, ventilation, and air conditioning costs.¹⁰ The implementation of dynamic windows, which modulate heat and light flow from the outside, reduces these building energy costs.¹¹⁻¹²

There are several strategies used to construct dynamic windows, which include electrochromic materials, 13-16 polymer-dispersed liquid crystals, 17-19 and automated blinds. 20,21 However, none of these approaches have been adopted on a large scale due to cost, durability, color, and switching speed issues, or the inability to support multiple tinting states.²²⁻²⁷ Reversible metal electrodeposition (RME) is an emerging technology for dynamic windows, which operates based on the deposition and dissolution of metal ions.^{6,28-30} RME windows are composed of a transparent conducting working electrode, such as tin-doped indium oxide (ITO), a counter electrode, and a gel or liquid electrolyte containing salts of colorless metal ions. 31-33 When a reducing potential is applied to the working electrode, the metal ions in the electrolyte are deposited on the surface of the ITO in their metallic form, thus darkening the window. At the same time, the counter electrode provides the other half of the redox reaction to balance charge. By changing the amount of time the voltage is applied to the window, the thickness of the metal electrodeposited on the ITO is controlled, thus resulting in a device with tunable optical transmission. When an oxidation potential is later applied to the working electrode, the metal is stripped off the ITO and turned back into ions, making the window more transparent. 34-36

RME dynamic windows have been shown to possess superior optical contrast and potentially faster switch times than other methods. ^{6,13,19,37} Metals have several intrinsic properties that make them ideal for dynamic windows. Metals are highly opaque in their elemental form. ^{38,39} This opacity results in the ability to block light effectively using films only tens of nanometers thick. ^{40,41} Additionally, many metals are chemically noble and color neutral. ^{32,42} Several relatively noble metals (Bi, Cu, Pb, Ag, and Au) have previously been reported for use in dynamic windows. ^{4,43-46} Recently, Zn has been investigated as a nonnoble alternative to these metals. ^{4,6,47}

We previously developed Zn RME electrolytes containing ZnCl₂, ZnBr₂, and sodium formate that have a high Coulombic efficiency of 99% and support a high contrast ratio of greater than 70%. And a several inherent advantages compared to other metals such as Bi, Cu, and Pb. Zn electrodeposits produce a black window in the opaque state, whereas Cu is red. In is also nontoxic, unlike Pb. Furthermore, unlike Ag and Au, Zn is inexpensive. Compared to Bi, which is only soluble in water at pH \leq 2 under standard conditions, Zn is soluble in water at higher pH values. Unlike highly acidic Bi electrolytes, these less acidic Zn electrolytes do not etch ITO, resulting in improved device shelf life. Sa,54

However, the standard reduction potential of -0.76 V vs. normal hydrogen electrode (NHE) of Zn means that it is substantially less noble than other metals used in dynamic windows.⁵² While the presence of coordinative ligands to form Zn complexes can shift the standard reduction potential, this standard reduction potential is negative enough that it indicates that from a thermodynamic perspective, water will be reduced to H₂ before Zn ions can become Zn metal.⁵⁵ However in many cases, the overpotential for H₂ evolution is much larger than that of Zn electrodeposition, which allows Zn deposition to occur prior to H₂ evolution.⁵⁶ Side

products of Zn reduction, ZnO and Zn(OH)₂, are formed on the surface of the working electrode during deposition under appropriate conditions. These species kinetically inhibit H₂ evolution at the working electrode. ^{47,57}

In this manuscript, we explore a new class of Zn electrolytes that employs sulfate anions. Supporting ions in Zn electrolytes have previously been demonstrated to dramatically affect the morphology of Zn electrodeposition by both changing the speciation of Zn complexes in the electrolyte and affecting the dynamics of metal nucleation and growth on the electrode. The morphology of the metal electrodeposits is an important parameter that dictates device switching speed because smoother electrodeposits block light more efficiently than rough ones. We were intrigued by battery literature demonstrating that ZnSO₄-based electrolytes supported batteries with long cycle lives. We find that the sulfate anion improves the Coulombic efficiency of the Zn electrolytes and also greatly influences the morphology of Zn electrodeposits. These studies will aid in the future development of robust Zn dynamic windows.

2. Experimental Section

Chemicals were obtained from commercial sources and used without further purification. Three-electrode experiments were performed and measured using a Zn metal foil (99.9%) as a reference electrode and a separate Zn metal foil as a counter electrode. ITO on glass was modified by spray coating a 3:1 vol. % dispersion of water and Pt nanoparticles (Sigma Aldrich, 3 nm in diameter) on ITO on glass substrates (Xinyan Technology, 15 Ω sq⁻¹). The Pt-modified ITO on glass substrates were then heated under air at 200°C for 20 minutes and were used as the working electrodes with a geometric surface area of 3 cm². The Pt nanoparticles serve as a seed layer that improves metal nucleation kinetics and electrodeposit uniformity as has been described previously.¹⁻⁵ Electrochemistry was conducted using a VSP-300 Biologic potentiostat. All CV

data presented are the second cycle unless otherwise stated. Transmission data were recorded with an Ocean Optics FLAME-S-VIS-NIR spectrometer with an Ocean Optics DH-mini UV-Vis-NIR light source.

For three-electrode spectroelectrochemical experiments, measurements were conducted in a 2 cm by 2 cm glass cuvette with 5 mL of electrolyte. A transmission value of 100% was defined as the electrolyte in the cuvette without the working electrode.

The compositions of various electrolytes are listed in the figure captions. Solutions were prepared by adding the appropriate solids to 20 mL of de-ionized water. The pH values of the solutions were then adjusted to 4.8 ± 0.3 with the conjugate acid of an electrolyte anion. For example, chloride-containing electrolytes were pH adjusted with HCl, while nitrate-containing electrolytes were pH adjusted with HNO₃. The solutions were next converted to gels by the addition of 2% wt. hydroxyethylcellulose (Sigma Aldrich, average $M_v \sim 90,000$) after stirring overnight. Electrolytes containing polyethylene glycol utilized the polymer with an average M_w of 1,500 (Sigma Aldrich).

For two-electrode 25 cm² dynamic windows, Cu tape with conductive adhesive was first placed along the edges of the Pt-modified ITO on glass to make uniform electrical connection to the perimeter of the working electrode. The counter electrode was comprised of a Zn mesh with a wire diameter of 3 mm and an interwire spacing of about 1 cm. The mesh was placed on top of a nonconductive glass backing. In future work, we will develop more aesthetically-pleasing Zn meshes that possess thinner metal grid lines that are more optically transparent. The development of thin metal grid lines, however, is outside the scope of this work, but they have been studied in other reversible metal electrodeposition systems previously.⁶¹ Butyl rubber (Solargain, Quanex, Inc.) was placed around the edges of the device stack to seal the two electrodes together with an

interelectrode spacing of about 5 mm. The gel electrolyte was then injected into the device stack through the butyl rubber sealant via a syringe. The outside surfaces of the completed dynamic window were cleaned with glass cleaner before performing the optical measurements. For window experiments, a transmission value of 100% was defined as open air. Transmission spectra were recorded in the center of the window and through an opening in the Zn mesh. However, some of the light from the light source was blocked by the mesh wires, which explains why the clear state transmission values for the 25 cm² dynamic window measurements are significantly less than those recorded in the three-electrode experiments.

Scanning electron microscope (SEM) images were obtained using a JOEL JSM-6010LA microscope with an operating voltage of 20 kV. X-ray diffraction (XRD) was conducted using a Bruker D2 X-ray Diffractometer. The electrodeposits for SEM and XRD analysis were formed as indicated in the figure captions.

3. Results and Discussion

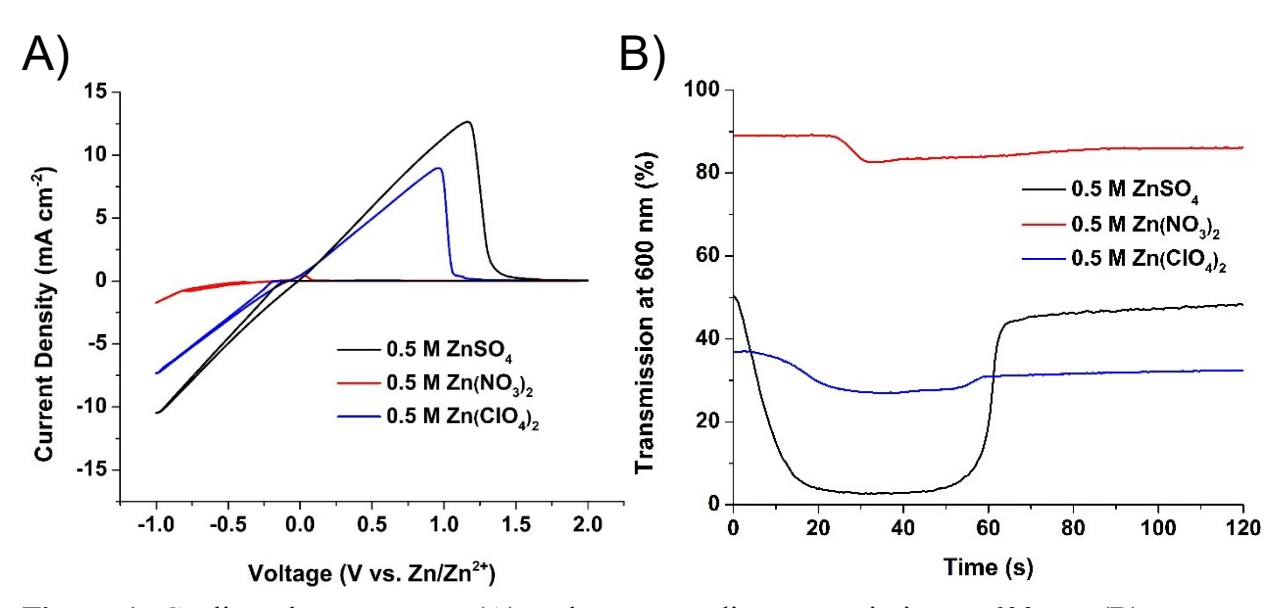


Figure 1: Cyclic voltammograms (A) and corresponding transmission at 600 nm (B) at a scan rate of 50 mV s⁻¹ of Pt-modified ITO working electrodes in electrolytes containing 0.5 M ZnSO₄ (black line), 0.5 M Zn(NO₃)₂ (red line), or 0.5 M Zn(ClO₄)₂ (blue line).

To study the electrochemical behavior of Zn and how the supporting anions can influence the electrodeposition and stripping processes, we selected three Zn compounds that have non-coordinating anions. Each experiment was done with the same molarity of metal ions to ensure that the only difference would be the anions. Because all three species are non-coordinating anions, we expected that all of the electrolytes would share general Zn deposition and stripping features. However, the results show important differences. While both the cyclic voltammograms (CVs) of ZnSO₄ and Zn(ClO₄)₂ contain prominent deposition and stripping features, the CV for Zn(NO₃)₂ possesses a relatively small amount of current (Figure 1A). In tandem with Zn electrodeposition, NO₃⁻ reduction to NO₂⁻ and NH₃ occurs at potentials more negative than -0.3 V. This finding matches previous studies of NO₃⁻ on Zn electrodes.²⁵ Furthermore, a CV in a 0.5 M NaNO₃ electrolyte without Zn²⁺ also exhibits reductive current at similar voltages, providing further evidence that NO₃⁻ reduction occurs (Figure S1). As a result, the NO₃⁻ reduction reaction inhibits the reversible Zn electrodeposition process.

The differences in the voltammetry also correspond to altered optical transmission of the electrodes during the CVs (Figure 1B). The electrode transmission using the Zn(NO₃)₂ electrolyte possesses the lowest change in transmission with a contrast ratio (defined as the difference between the maximum and minimum transmission values during one cycle) of less than 10% during deposition (Figure 1B, red line) due to the inhibitory effect of NO₃⁻. Similarly, the experiment with Zn(ClO₄)₂ exhibits an electrode contrast ratio of only slightly greater than 10% (Figure 1B, blue line). In addition to its non-coordinating nature, ClO₄⁻ is an electrochemically inert anion unlike NO₃⁻. Previous studies of RME electrolytes with Bi and Cu have demonstrated that ClO₄⁻ does not actively participate in the metal deposition and stripping processes.^{5,36} Therefore, the voltammetry and transmission results for the Zn(ClO₄)₂ can be

interpreted as arising from solely Zn electrochemistry. Interestingly, the transmission curve for the ZnSO₄ possesses much greater optical contrast (>45%) than the other two electrolytes (Figure 1B, black line). Furthermore, the electrode with the ZnSO₄ electrolyte is the only one that reaches its original transmission during Zn stripping. The finding that the ZnSO₄ electrolyte supports high current density and good optical contrast and reversibility demonstrates that even though SO₄²⁻ is a non-coordinating anion, there is a beneficial secondary effect of SO₄²⁻ that aids in Zn spectroelectrochemistry. The subsequent experiments in this manuscript explore this hypothesis.

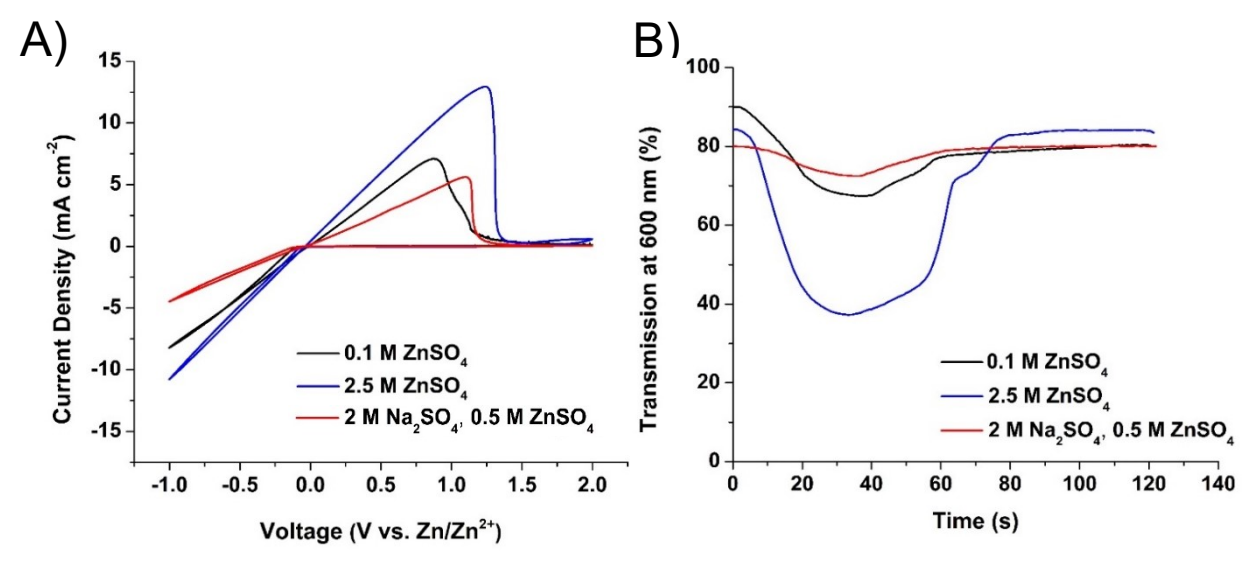


Figure 2: Cyclic voltammograms (A) and corresponding transmission at 600 nm (B) at a scan rate of 50 mV s⁻¹ of Pt-modified ITO working electrodes in electrolytes containing 0.1 M ZnSO₄ (black line), 2.5 M ZnSO₄ (blue line), or containing 2.0 M sodium formate and 0.5 M ZnSO₄ (red line).

In Figure 1B and all subsequent analogous figures, the initial transmission values of the electrolytes are different. These discrepancies result from the fact that the data were taken from the second CV cycles, and so any irreversibility from the first cycle resulted in a decreased starting electrode transmission. We analyze the second cycles of the CVs because nucleation occurs more prominently on the ITO working electrode during the first CV cycle, which

complicates analysis. In this way, the second CV cycle is more representative of the general spectroelectrochemical behavior of the electrolytes.

After identifying the beneficial effects of SO₄²⁻, we evaluated the spectroelectrochemistry of the ZnSO₄ electrolyte at two additional concentrations (Figure 2, black and blue lines). Before explaining the results, we note that the electrolytes in Figure 2 are liquid electrolytes, while those in all other figures in the manuscript are gels formed by the addition of 2 wt. % hydroxyethylcellulose. Liquid electrolytes were analyzed in this data set because ZnSO₄ is not soluble in gels formed at concentrations of 2.5 M or higher. Compared to the 0.1 M electrolyte, the electrode using the 2.5 M ZnSO₄ electrolyte exhibits a greater current density during both deposition and stripping, as well as better optical properties including greater contrast and reversibility. This finding is expected because a greater quantity of Zn ions increases the current associated with Zn electrochemistry.

However, in our discussion of Figure 1, we identified that SO_4^{2-} influences Zn electrodeposition, and therefore we wondered if the enhanced Zn deposition and stripping current with 2.5 M ZnSO₄ is attributed solely to the increased Zn²⁺ concentration. To determine the effects of Zn²⁺ and SO_4^{2-} , we performed a CV with 2 M Na₂SO₄ and 0.5 M ZnSO₄ (Figure 2A, red line). This electrolyte contains an equal molarity of SO_4^{2-} ions, but a reduced amount of Zn²⁺, 0.5 M, as compared to the 2.5 M ZnSO₄ electrolyte. Because the CV of the electrode with the Na₂SO₄-ZnSO₄ electrolyte possesses less current than the 2.5 M ZnSO₄ electrolyte, we conclude that the increased concentration of Zn²⁺ does indeed result in faster Zn plating.

Furthermore, the transmission curve of the 2.5 M ZnSO₄ liquid electrolyte (Figure 2B, blue line) exhibits similar optical contrast (>45%) as the 0.5 M ZnSO₄ gel electrolyte (Figure 1B, black line). Previous studies with Bi-Cu RME systems have shown that electrolytes containing

hydroxyethlycellulose facilitate higher contrast ratios than liquid electrolytes due to their ability to produce more compact metal electrodeposits.⁵ The observation that the two electrolyte concentrations exhibit similar optical contrasts demonstrates that while the increased concentration of Zn²⁺ results in increased current density in the 2.5 M electrolyte, the absence of the gel is detrimental. These two processes effectively cancel each other out, giving the 2.5 M liquid electrolyte and 0.5 M gel electrolyte equal optical contrasts. However, the gel electrolyte has the advantage of being more suited to the construction of practical dynamic windows. Because 2.5 M ZnSO₄ is not soluble in the gel electrolyte, we chose to study derivatives of the 0.5 M ZnSO₄ gel electrolyte for the remainder of this manuscript.

Our next objective was to identify if there were any additional supporting ions that could be added to improve the electrolyte performance. Previous studies have shown that sodium formate improves the performance of Zn RME electrolytes that do not contain SO_4^{2-47} This improvement is due in part to the basicity of formate (pK_a = 3.7), which increases Zn stripping kinetics through the formation of soluble Zn formate complexes at the ITO-electrolyte interface. In addition to its basicity, the sterically unencumbered structure of formate allows enhanced nucleophilic attack on electrodeposited Zn as compared to other carboxylates such as acetate. It was also shown that halides aid Zn stripping due to the formation of stable Zn-halogen coordination complexes.⁴⁷ Based on this previous work, we decided to study ZnSO₄ electrolytes with the addition of sodium formate and Zn halides. Due to the insolubility of ZnF₂ and the ease with which Γ is oxidized to Γ , we focused our studies on ZnCl₂ and ZnBr₂.

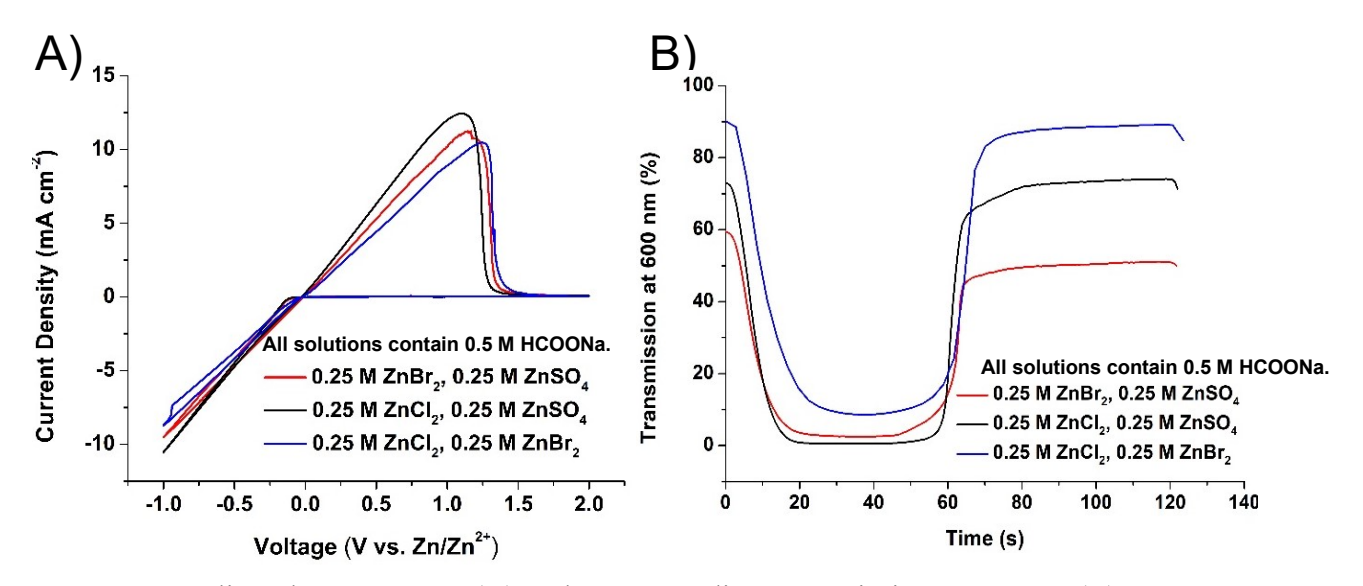


Figure 3: Cyclic voltammograms (A) and corresponding transmission at 600 nm (B) at a scan rate of 50 mV s⁻¹ of Pt-modified ITO working electrodes in electrolytes containing 0.5 M sodium formate and 0.25 M ZnSO₄ and 0.25 M ZnCl₂ (black line), 0.25 M ZnSO₄ and 0.25 M ZnBr₂ (red line), or 0.25 M ZnBr₂ and 0.25 M ZnCl₂ (blue line).

Figure 3 shows CVs and the corresponding electrode transmissions for the ZnCl₂-ZnSO₄-HCOONa and ZnBr₂-ZnSO₄-HCOONa electrolytes as compared to the previously studied ZnCl₂-ZnBr₂-HCOONa electrolyte.⁴⁷ While the general features of the CVs among the three electrolytes are similar (Figure 3A), there are important differences in the optical reversibility of the systems (Figure 3B). The ZnCl₂-ZnSO₄-HCOONa and the ZnCl₂-ZnBr₂-HCOONa electrolyte both possessed similarly large optical contrast ratios, and the electrode transmissions for both electrolytes return to their initial values during stripping. These results indicate that the ZnCl₂-ZnSO₄-HCOONa electrolyte developed in this manuscript is comparable in terms of its spectroelectrochemical performance to the previously developed ZnCl₂-ZnBr₂-HCOONa system.⁴⁷ Furthermore, the electrode using the ZnBr₂-ZnSO₄ electrolyte exhibits the lowest contrast ratio (<60%) and also is the least optically reversible. Previous results with ZnBr₂-HCOONa RME electrolytes demonstrate that bromide favors the formation of large heterogeneous particles that are more difficult to strip than films of smaller, more homogenous

deposits.⁴⁷ Having established that the ZnCl₂-ZnSO₄-HCOONa electrolytes possess promising spectroelectrochemical attributes for dynamic windows, we next performed systematic compositional studies to understand the function of each electrolyte component and their relation to each other.

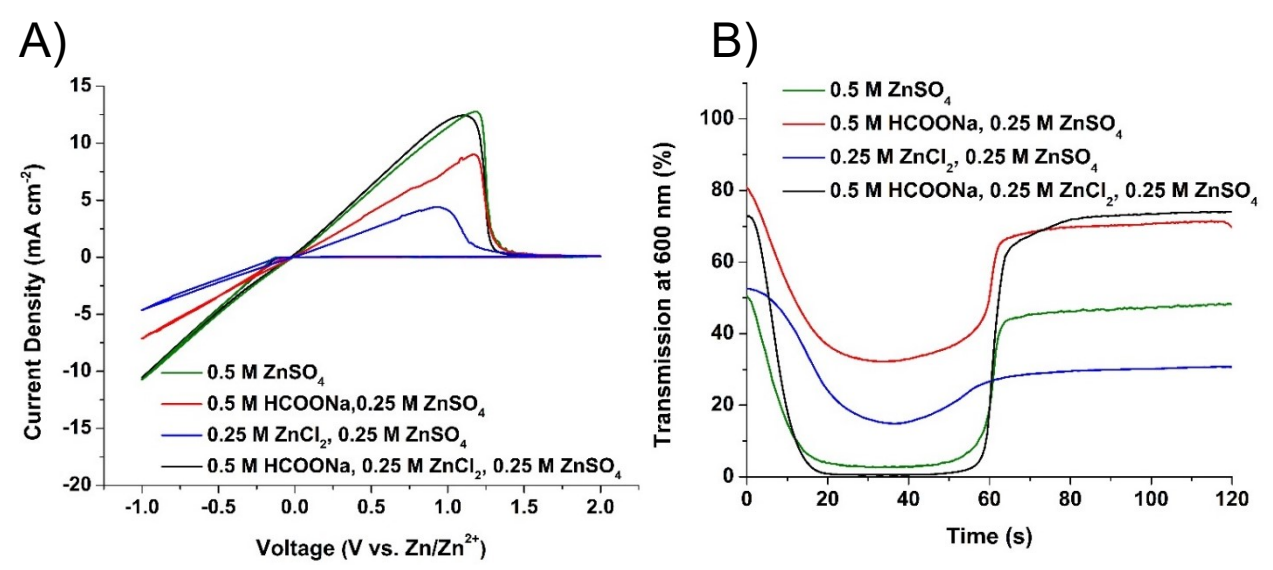


Figure 4: Cyclic voltammograms (A) and corresponding transmission at 600 nm (B) at a scan rate of 50 mV s⁻¹ of Pt-modified ITO working electrodes electrolytes containing 0.5 M ZnSO₄ (green line), 0.5 M sodium formate and 0.5 M ZnSO₄ (red line), 0.25 M ZnCl₂, and 0.25 M ZnSO₄ (blue line), or 0.5 M sodium formate, 0.25 M ZnSO₄, and 0.25 M ZnCl₂ (black line).

As a point of comparison, the spectroelectrochemistry of the ZnSO₄ electrolyte is reproduced as the green lines in Figure 4. The CV of the electrolyte with formate added exhibits reduced current density for both Zn electrodeposition and stripping (Figure 4A, red line). The corresponding electrode transmission also possesses lower contrast and less reversibility (Figure 4B, red line) as compared to ZnSO₄ only. Furthermore, the addition of chloride to the ZnSO₄ electrolyte results in even less current density in the CV and less optical contrast and reversibility (Figure 4, blue line). However, the addition of both formate and chloride to the ZnSO₄ electrolyte results in a similar CV (Figure 4A, black line) as the ZnSO₄ only. The electrode in this electrolyte also has excellent optical reversibility and the greatest contrast ratio of around

70% compared to about 50% for ZnSO₄ only. The improved spectroelectrochemical properties of the ZnCl₂-ZnSO₄-HCOONa are surprising given that individual additions of formate or chloride to ZnSO₄ produced inferior performance. These results indicate that formate and chloride together with the ZnSO₄ have a beneficial synergetic effect. Later in the manuscript, we demonstrate that this synergy is related to the morphology of the electrodeposits formed from this electrolyte.

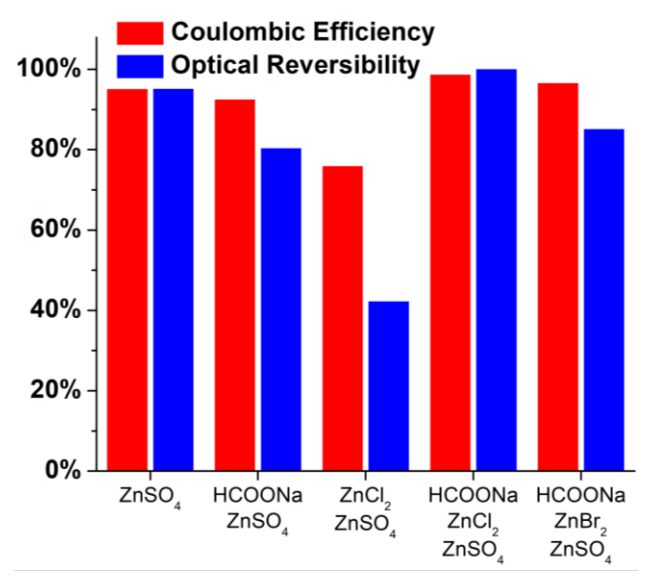


Figure 5: Coulombic efficiencies of the CVs (red bars) and corresponding optical reversibilities of electrodes (blue bars) using sulfate electrolytes with various compositions.

The improved spectroelectrochemical properties of the $ZnCl_2$ - $ZnSO_4$ -HCOONa electrolyte are also evident in the Coulombic efficiency and optical reversibility of the electrodes in the various electrolytes (Figure 5). Here, the Coulombic efficiency is defined as the amount of charge passed during Zn stripping divided by the amount of charge passed during Zn electrodeposition. The optical reversibility of the electrode is defined as the ratio of the transmission changes during the deposition and stripping processes during the CV cycle, and is given by Equation 1, where $T_{initial}$ is the transmission at the beginning of the CV, T_{final} is the

transmission at the end of the CV, and T_{min} is the minimum transmission measured during the CV.

$$\frac{T_{final} - T_{min}}{T_{initial} - T_{min}}$$
 (Equation 1)

The ideal value for both the Coulombic efficiency and optical reversibility is 100%, which would indicate that the electrolyte supports complete electrochemical and optical reversibility, respectively. The data in Figure 5 demonstrate that across the five electrolytes evaluated there is a correlation between Coulombic efficiency and optical reversibility. In particular, the ZnCl₂-ZnSO₄-HCOONa electrolyte possesses the highest Coulombic efficiency (99%) and optical reversibility (100%). These values are significantly higher than those for the electrolytes containing the individual components (ZnSO₄, ZnSO₄-HCOONa, and ZnCl₂-ZnSO₄).

Compared to the ZnCl₂-ZnSO₄-HCOONa electrolyte, a ZnBr₂-ZnSO₄-HCOONa electrolyte has only a slightly diminished Coulombic efficiency (97%), but the corresponding optical reversibility decreases significantly (85%). This decreased optical reversible likely arises from morphological changes induced by the presence of Br⁻, which inhibits electrodeposit stripping. Indeed, previous work with related ZnBr₂ electrolytes has shown that Br⁻ induces the formation of large heterogeneous Zn particles.⁴⁷ These larger particles have fewer points of contact with the electrode and thus generally exhibit slower stripping kinetics. Next, we more thoroughly investigate how electrodeposit morphology impacts optical switching speed.

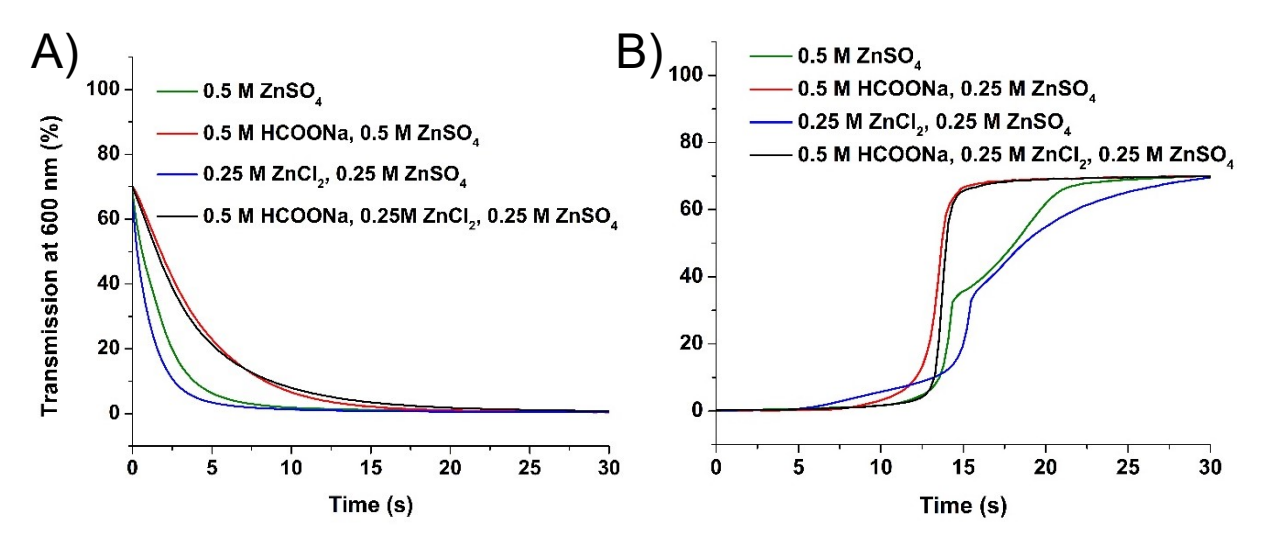


Figure 6: Transmission at 600 nm of the working electrode during Zn electrodeposition at -1.0 V (A) and stripping at +2.5 V (B) in electrolytes containing 0.5 M ZnSO₄ (green line), 0.5 M sodium formate and 0.5 M ZnSO₄ (red line), 0.25 M ZnCl₂ and 0.5 M ZnSO₄ (blue line), or 0.5 M sodium formate, 0.25 M ZnSO₄, and 0.25 M ZnCl₂ (black line). To elicit Zn electrodeposition, chronoamperometry was conducted at -1.0 V until the transmission at 600 nm reached 1%. Next, Zn stripping was conducted at +2.5 V for 30 s.

We evaluated the speed of electrode darkening and stripping during Zn deposition by measuring the time required to reach and return from 1% transmission in each electrolyte (Figure 6). This investigation was also coupled with SEM images of each electrolyte's electrode during deposition (Figure 7). The electrode using the electrolyte containing only ZnSO₄ decreases to about 1% transmission in less than 10 s (Figure 6A, green line). During metal stripping, the electrode transmission returns most of the way to its original 70% value within 20 s (Fig 6B, green line). The short amount of time that the electrode takes to reach 1% transmission can be explained by its SEM images (Figures 7A and S2A). The dark regions of the images show that the ZnSO₄ electrolyte produces a smooth, fairly uniform film of electrodeposits that is capable of blocking light effectively. However, the images also reveal lighter particles that possess a more dendritic structure. Due to their lower surface coverage, these dendritic structures do not significantly aid in reducing electrode transmission, but they hinder electrode stripping kinetics in comparison to the other tested Zn electrolytes.

The addition of formate to the electrolyte substantially increases the amount of time needed for the electrode to reach 1% transmission (Figure 6A, red line). Despite the slower darkening speed, this electrolyte results in the fastest bleaching time of the four electrolytes tested (Figure 6B, red line). The electrodeposited film on the electrode with this ZnSO₄-HCOONa electrolyte is comprised of loosely-packed particles (Figures 7B and S2B). The spaces between the electrodeposited particles allow light to pass through, which explains the slower electrode darkening time. However, the relatively smaller size of the particles allows for more surface contact with the electrode, which enables faster stripping kinetics.

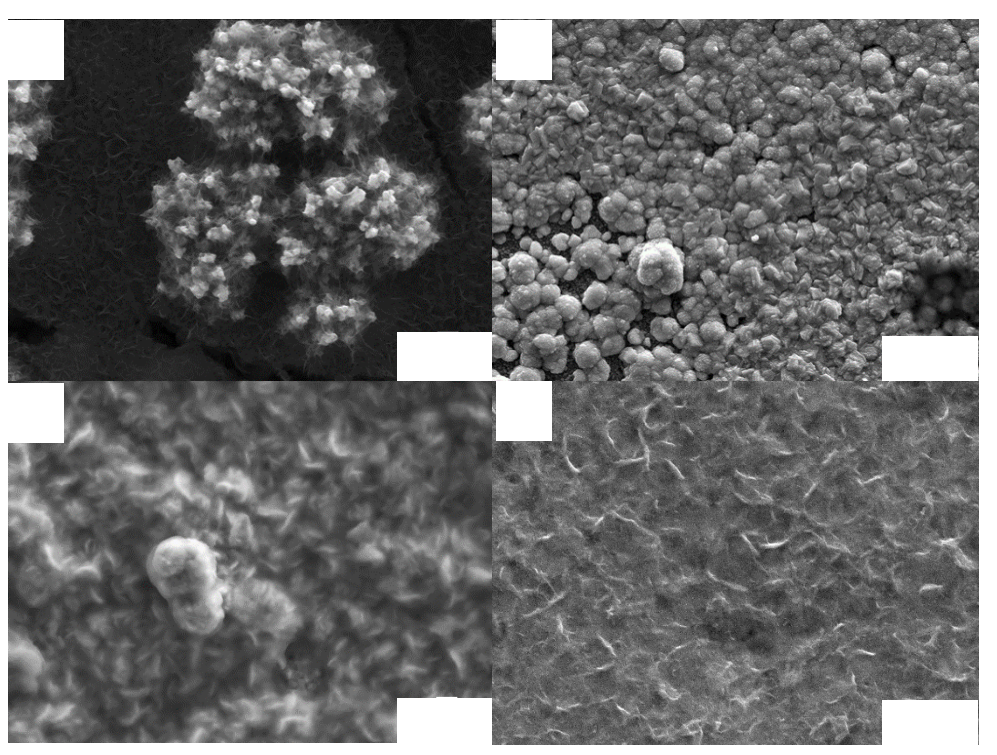


Figure 7: Scanning electron microscopy images of Zn electrodeposits obtained after a linear sweep voltammogram from 0 V to -1 V at 5 mV s⁻¹ in electrolytes containing 0.5 M ZnSO₄ (A), 0.5 M sodium formate and 0.5 M ZnSO₄ (B), 0.25 M ZnSO₄ and 0.25 M ZnCl₂ (C), and 0.5 M sodium formate, 0.25 M ZnSO₄, and 0.25 M ZnCl₂ (D).

The electrodeposits produced from the ZnCl₂-ZnSO₄ electrolyte consist of larger and denser particles than those generated using the ZnSO₄-HCOONa electrolyte (Figures 7C and S2C). This film has fewer and smaller gaps, and thus the electrode possesses the fastest

darkening time (Figure 6A, blue line), but the large size of the particles also results in the slowest bleaching time (Figure 6B, blue line). The transmission profiles during stripping of the electrodeposits from both the ZnSO₄ and ZnCl₂-ZnSO₄ electrolytes possess a shoulder at around 15 s. We hypothesize that this shoulder occurs because these electrodeposits contain particles with two distinct morphologies, each of which exhibits different stripping kinetics.

The full ZnCl₂-ZnSO₄-HCOONa electrolyte possesses similar transmission profiles (Figure 6, black line) as the ZnSO₄-HCOONa electrolyte during both deposition and stripping. SEM images reveal that the film on the electrode from the ZnCl₂-ZnSO₄-HCOONa electrolyte contains a sparse coverage of small, thin particles. This morphology is not as effective at blocking light, which explains the relatively slow electrode darkening time with this electrolyte (Figure 6A, black line). However, the small particles are conducive to rapid metal stripping (Figure 6B, black line). The fast stripping speed facilitated by this morphology combined with this electrolyte's high Coulombic efficiency (99%) make the ZnCl₂-ZnSO₄-HCOONa electrolyte a promising candidate for practical Zn-based dynamic windows. Therefore, we studied the long-term cyclability of dynamic windows using this electrolyte.

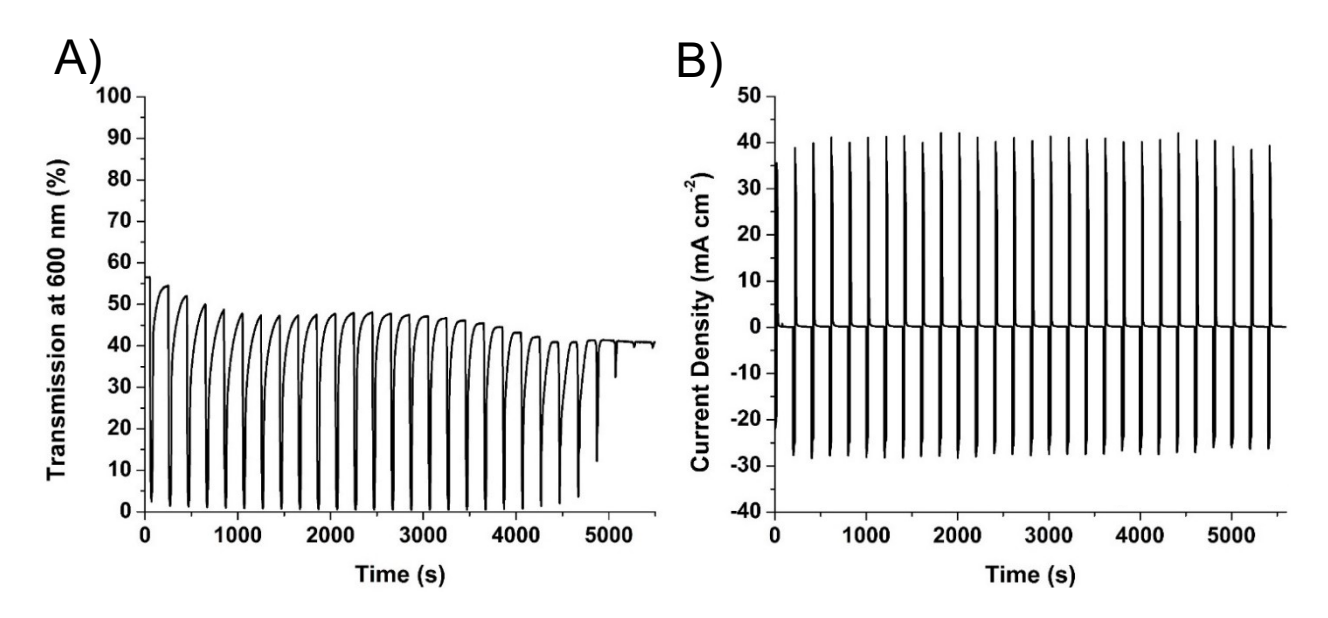


Figure 8: Transmission at 600 nm (A) and chronoamperometry (B) of a 25 cm² Zn dynamic window using the ZnCl₂-ZnSO₄-HCOONa electrolyte. The device was switched at -1.4 V for 20 s to induce metal electrodeposition and +1.75 V for 180 s to elicit metal stripping.

Figure 8 shows the optical transmission and chronoamperometry of a 25 cm² twoelectrode dynamic window with the ZnCl₂-ZnSO₄-HCOONa electrolyte over the course of 28
cycles. The low starting transmission of the window of about 56% is due to the mesh counter
electrode, which blocks some of the light passing through the window. If commercially adopted,
RME windows could utilize meshes with thinner diameter wires that are invisible to the human
eye.⁶² The window was, however, able to achieve a contrast ratio of about 50% during its first
cycle (Figure 8A). This high contrast ratio is complimented by nearly complete optical
reversibility. Furthermore, these cycling properties are more or less retained during the next 21
cycles. During further cycling, however, the contrast decreases precipitously, resulting in a less
than 3% contrast ratio during the final cycle. Interestingly, the declining contrast ratio is not
accompanied by a similar decline in the current density during chronoamperometry (Figure 8B).
This result suggests that a change in morphology or composition of the electrodeposit instead
occurs, as opposed to degradation of the ITO working electrode.

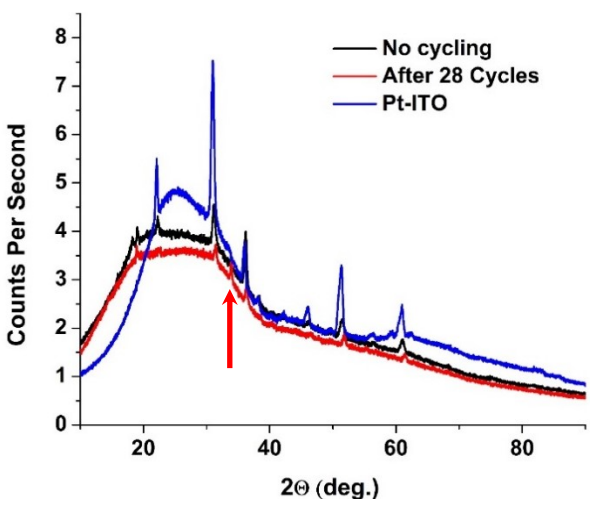


Figure 9: X-ray diffraction spectra of Pt-modified ITO working electrodes before assembly (blue line) and after incorporation in a 25 cm² Zn dynamic windows using the ZnCl₂-ZnSO₄-

HCOONa electrolyte without cycling (black line) and after 28 cycles (red line). The red arrow indicates the new peak at 34°, which is ascribed to Zn₄(OH)₆SO₄, that appears after cycling.

To investigate if the composition of the ITO working electrode changed during cycling, we performed XRD at different states of the Zn dynamic window (Figure 9). The XRD spectrum of the initial Pt-modified ITO electrode before window assembly (blue line) has characteristic peaks at 22°, 31°, 36°, 51°, and 61°, which are ascribed to the (211), (222), (400), (440), and (622) crystalline facets, respectively, of In₂O₃ in the ITO.⁶³ We then measured the XRD spectrum the Pt-modified ITO electrode after it was cycled 28 times in a 25 cm² Zn dynamic windows using the ZnCl₂-ZnSO₄-HCOONa (red line). When comparing the XRD spectrum of this cycled electrode with the pristine Pt-modified ITO spectrum, the cycled spectrum possesses a new peak at 34° (red arrow). Based on published XRD analysis of the interaction of Zn²⁺ and SO₄²⁻ ions, this peak could be due to Zn₄(OH)₆SO₄.⁶⁴ Alternatively, this peak could be assigned to ZnO. The published XRD spectra of both Zn₄(OH)₆SO₄ and ZnO possess a peak around 34°, ⁶⁵ and because this peak is the only new one to arise in the spectrum of the cycled electrode, it is difficult to distinguish between the two species. To confirm that this peak is a result of cycling, we recorded an additional XRD spectrum of a Pt-modified ITO electrolyte that rested at open circuit potential in a non-cycled window for the same amount of time as it took to switch the cycled electrode 28 times (black line). Because there is no peak at 34° for this sample, ZnO or Zn₄(OH)₆SO₄ must be a product of electrochemical cycling, not simply electrolyte immersion.

We hypothesize that the side production of Zn₄(OH)₆SO₄ (alternatively expressed as (Zn(OH)₂)₃ZnSO₄) during window cycling could, at least in part, be responsible for the deterioration in optical contrast seen in Figure 8A. Previous work on cycling dynamic windows using other Zn electrolytes without SO₄²⁻ demonstrated that Zn(OH)₂ accumulates on the ITO

working electrode and is also a cause of optical contrast degradation during cycling.⁴⁷ In both cases, an alkaline Zn(OH)₂-based species is produced.

To further test the hypothesis that alkaline Zn(OH)₂ accumulates during cycling, we used acid immersions to see if cleaning the electrode would restore the performance of the electrode. Towards this end, we cycled a Pt-modified ITO working electrode in a three-electrode spectroelectrochemical cell using chronoamperometry. This setup allowed us to easily remove the working electrode to immerse it in acid in an attempt to chemically dissolve accumulated Zn(OH)₂. The electrode was subsequently washed thoroughly with water to remove any residual acid before it was reintroduced into the Zn electrolyte for further cycling. For these studies, we used the ZnCl₂-ZnBr₂-HCOONa electrolyte with 2 wt. % polyvinyl alcohol (PVA), which exhibits enhanced cycling durability. The PVA has been shown to produce a more uniform and smooth electrodeposit morphology in other RME systems, which improves cycling durability. Indeed, cycling durability is significantly reduced without PVA even with a seven-minute strpping time (Figure S3).

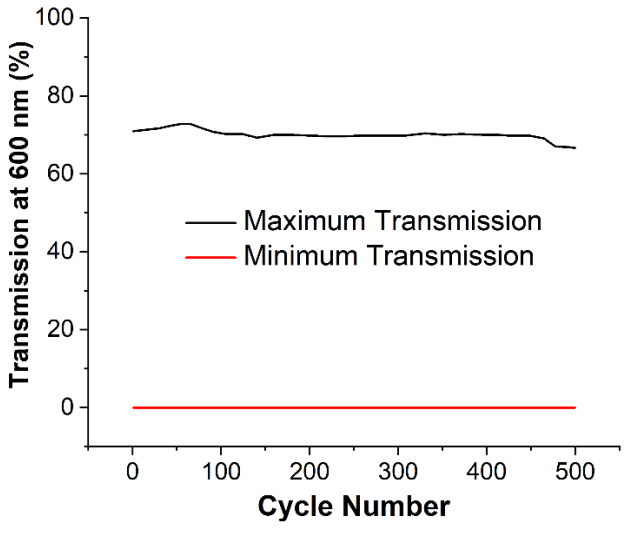


Figure 10: Maximum (black line) and minimum (red line) transmission at 600 nm of a Pt-modified ITO working electrode during chronoamperometry cycles. For each cycle, the voltage was held at -1.4 V for 12 s to induce electrodeposition followed by +1.75 V for 7 min to elicit

stripping. After every 100 cycles, the electrode was subjected to an acid immersion step as explained in the text.

Figure 10 shows the results of the acid-immersion cycling experiments over the course of 500 cycles. After every 100 cycles, the electrode was placed in 1 M HCl for 5 minutes and washed with water before cycling continued in the ZnCl₂-ZnBr₂-HCOONa electrolyte. The acid immersion steps prevented the decline in optical contrast ratio seen previously in Zn dynamic windows. A seven-minute stripping time was used to ensure complete optical reversibility throughout the course of each block of 100 cycles. A shorter stripping time, for example of one minute, results in optical irreversibility over 100 cycles regardless of whether PVA is in the electrolyte (Figures S4-S5).

Taken together, these results provide strong evidence that a Zn(OH)₂-based surface layer is responsible for poor long-term electrochemical cycling of Zn dynamic windows. In future work, we will focus on suppressing or eliminating the accumulation of Zn(OH)₂ without the acid immersion steps to increase Zn dynamic window cycle life. We next describe the use of a different polymer additive, polyethylene glycol (PEG), as one strategy to increase the cycleability of devices based on reversible Zn electrodeposition.

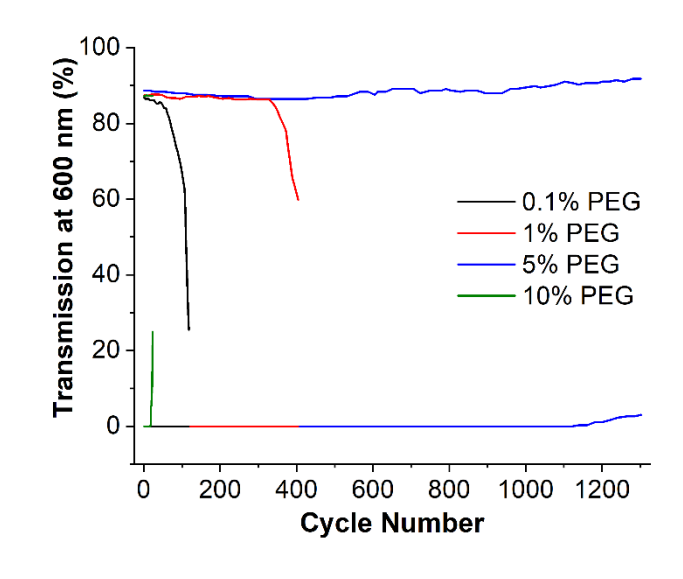


Figure 11: Maximum and minimum transmission at 600 nm of Pt-modified ITO working electrodes during chronoamperometry cycles using electrolytes containing 0.25 M ZnBr₂, 0.25 M ZnCl₂, and 0.5 M sodium formate with 0.1 wt. % (black line), 1 wt. % (red line), 5 wt. % (blue line), and 10 wt. % (green line) PEG. For each cycle, the voltage was held at -0.8 V for 15 s to induce electrodeposition followed by +2.5 V for 55 s to elicit stripping.

In our attempt to increase the cycle life of Zn-based windows, we were inspired by previous work on Zn batteries in which the inclusion of PEG extends battery cycleability. ⁶⁶ As we previously discussed above, polymers can improve both the optical contrast and lifespan of RME windows. ⁵ We engaged in a systematic study to investigate the impact that PEG could have on a window as a function of the amount of polymer in the electrolyte. The addition of 0.1 wt. % PEG to the ZnCl₂-ZnBr₂-HCOONa electrolyte (Figure 11, black line) resulted in a system that was able to reach less than 0.1% minimum transmission during each cycle. However, these steady minimum values were accompanied by an almost immediate steep decline in the maximum transmission of the ITO electrode from greater than 80% to less than 30% transmission in fewer than 100 cycles. We hypothesize that the low quantity of PEG favors the accumulation of ZnO and Zn(OH)₂ side products during cycling, which impede electrodeposit stripping kinetics as has been demonstrated previously in the electrolyte without PEG. ⁴⁷

Increasing the quantity of PEG in the electrolyte to 1 wt. % enabled the system to maintain a high maximum transmission and low minimum transmission for more than 300 cycles (Figure 11, red line). Further increasing the PEG content to 5 wt. % yielded a system that cycled more than 1,100 times with less than 0.1% minimum transmission and greater than 80% maximum transmission (Figure 11, blue line). These results show that the addition of PEG to the electrolyte can greatly extend the reversibility of Zn electrodeposition. The cycle life, however, significantly decreases to less than 20 cycles when the concentration of PEG is increased to 10% wt. Unlike the other PEG electrolytes, instead of the maximum transmission of the ITO electrode

decreasing, it is the minimum transmission of the ITO electrode that degrades during cycling, indicating that the high concentration of PEG inhibits Zn electrodeposition kinetics. As a whole, these results demonstrate that there is an optimal concentration of PEG (i.e. about 5 wt. %) that is most effective at enhancing the reversibility of Zn electrodeposition.

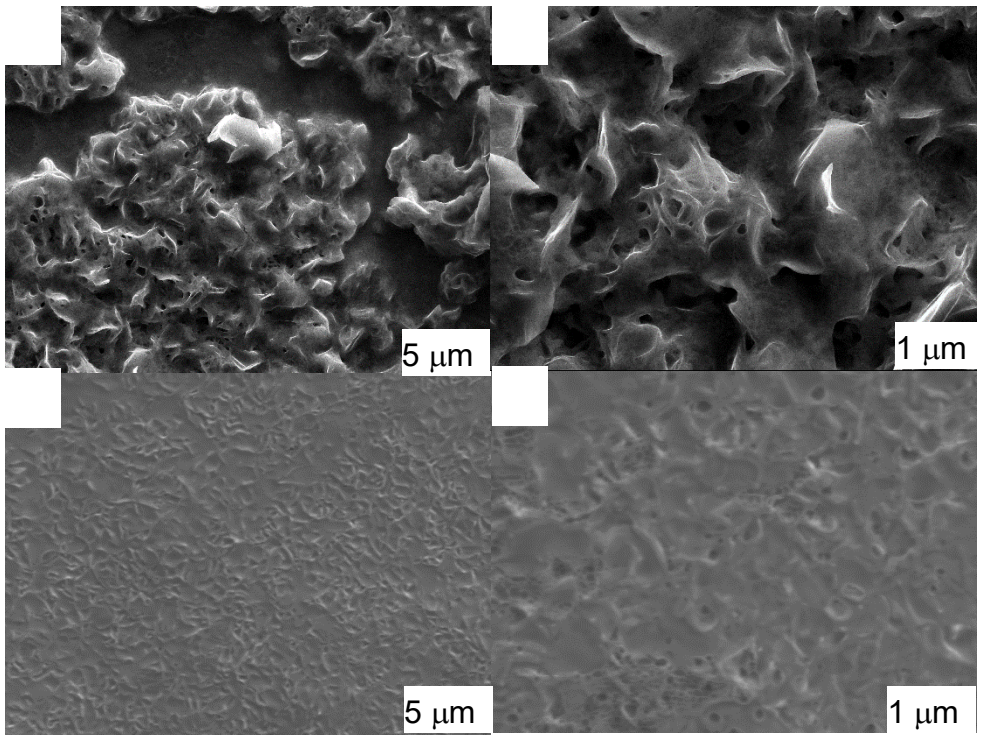


Figure 12: Scanning electron microscopy images of Zn electrodeposits obtained after chronoamperometry at -0.8 V for 15 s in electrolytes containing 0.25 M ZnBr₂, 0.25 M ZnCl₂, and 0.5 M sodium formate without (A, B) and with 5 wt. % PEG (C, D).

To investigate the origin of the enhanced cycle life in the presence of 5 wt. % PEG, we conducted SEM and XRD analysis. SEM images show that the Zn electrodeposits formed using the electrolyte without PEG are nonuniform and loosely packed (Figures 12A and 12B). The gaps in this morphology are inefficient at blocking light, which hampers the switching speed and minimum attainable transmission of the device. By comparison, the morphology of the electrodeposits produced from the electrolyte with PEG is much more uniform and densely packed (Figures 12C and 12D).

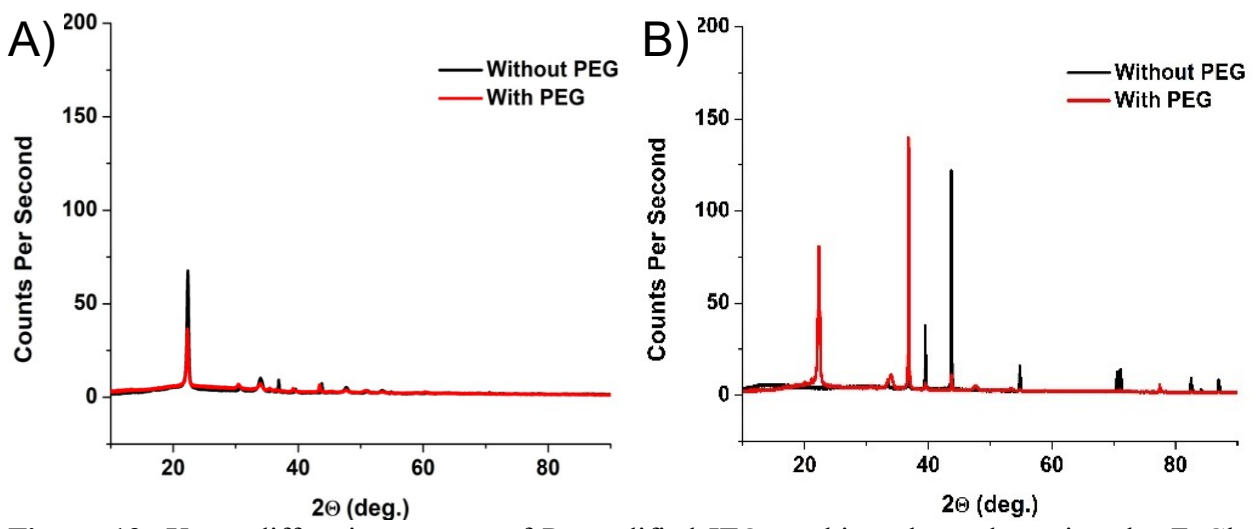


Figure 13: X-ray diffraction spectra of Pt-modified ITO working electrodes using the ZnCl₂-ZnBr₂-HCOONa electrolyte without (black lines) and with (red lines) 5 wt. % PEG after deposition at -0.8 V for 15 s (A) and after 100 cycles using -0.8 V for 15 s and 2.5 V for 55 s ending on deposition (B).

Using XRD, we also analyzed the composition of electrodeposits generated from electrolytes with and without PEG before and after cycling. For both electrolytes, the XRD spectra of electrodeposits produced on fresh electrodes display a prominent peak at about 23°, which is due to Zn(OH)₂ (Figure 13A).⁶⁷ In contrast, the XRD spectra of the electrodeposits after 100 switching cycles differ dramatically with and without PEG (Figure 13B). Without PEG, the most intense peak in the spectrum appears at around 43°, which is ascribed to the metallic Zn(101) crystal facet (Figure 13B, black line).⁶⁸ Previous work has shown that the (101) face is dominant in Zn when electrodeposits have a dendritic morphology, similar to those we observed in the SEM images (Figures 12A and 12B).^{69,70} However, with PEG, the most intense peak in the spectrum is positioned at 38°, which is due to the Zn(002) facet (Figure 13B, red line). In Zn batteries, the presence of this (002) facet is correlated with enhanced cycleability and the formation of prismatic-like deposits that resemble those produced on ITO in this work (Figure S6). During metal electrodeposition, the absorption of PEG on the surface of Zn decreases nucleation compared to growth.⁶⁸ With a decreased nucleation rate, dendrite formation is

suppressed. This mechanism results in a Zn morphology with increased uniformity, which enhances cycle life. Taken together, these results are yet another instance presented in this manuscript of how the morphology of Zn electrodeposits can be tuned based on the chemical composition of the electrolyte, which in turn affects the reversibility of Zn electrodeposition systems.

4. Conclusions

In this manuscript, we study Zn RME dynamic window electrolytes by systemically studying the effect non-coordinating anions, primarily SO₄²-, have on reversible Zn electrodeposition and dissolution. By comparing the morphology, compositions, optical reversibility, current density, and Coulombic efficiency of different combination of Zn electrolytes, we were able to build a connection between the anions and the spectroelectrochemical properties of the electrolytes. We established a relationship between the morphology and the optical reversibility of Zn electrodeposition and stripping. We then applied these results to build a 25 cm² dynamic window, which showed excellent optical contrast. Although the cycling durability of these windows were poor, we discovered that the accumulation of Zn(OH)₂ species on the ITO electrode is responsible for optical degradation. We showed the elimination of these accumulated species greatly enhances the long-term cyclability of the windows. Lastly, we further demonstrated that the addition of PEG to the electrolyte greatly extends device cycle life. For all of these reasons, Zn window are promising candidates for future practical RME dynamic windows, and they warrant further research.

Associated Content

The Supporting Information is available free of charge.

Additional SEM images, transmission data, and chronoamperometry data of the reversible Zn electrodeposition systems.

Author Contributions

C. J. B. and M. D. M. conceived the project. D. C. M., M. V. L. A. A. T., and H. P. performed the experiments. D. C. M. and C. J. B. analyzed the data. D. C. M., M. D. M., and C. J. B. wrote the paper. All authors have given approval to the final version of the manuscript.

Conflict of Interest Statement

Madu and Barile have filed a provisional patent application related to this work. McGehee is a co-founder of Tynt Technologies, a company commercializing dynamic windows. The other authors declare no conflicts of interests.

Acknowledgments

This material is based upon work supported by the National Science Foundation under Grant No. ECCS2127308. We acknowledge the Share Instrumentation Laboratory in the Department of Chemistry at UNR. We gratefully acknowledged the support of National Science Foundation (CHE-1429768) for purchasing the X-ray diffractometer. SEM-EDX analysis was performed in the Mackay Microbeam Laboratory at UNR, and we thank J. Desormeau for his kind assistance.

References

- 1. Islam, S. M.; Fini, C. N.; Barile, C. J. Dynamic Windows Based on Reversible Metal Electrodeposition with Enhanced Functionality. *J. Electrochem. Soc.*, **2019**, *166*, D333-D338.
- 2. Islam, S. M.; Hernandez, T. S.; McGehee, M. D.; Barile, C. J. Hybrid Dynamic Windows using Reversible Metal Electrodeposition and Ion Insertion. *Nat. Energy*, **2019**, *4*, 223-229.
- 3. Islam, S. M.; Barile, C. J. Dual Tinting Dynamic Windows Using Reversible Metal Electrodeposition and Prussian Blue. *ACS Appl. Mater. Inter.*, **2019**, *11*, 40043-40049.
- 4. Barile, C. J.; Slotcavage, D. J.; Hou, J.; Strand, M. T.; Hernandez, T. S.; McGehee, M. D. Dynamic Windows with Neutral Color, High Contrast, and Excellent Durability using Reversible Metal Electrodeposition. *Joule*, **2017**, *1*, 133-145.

- 5. Strand, M. T.; Hernandez, T. S.; Danner, M. G.; Yeang, A. L.; Jarvey, N.; Barile, C. J.; McGehee, M. D. Polymer Inhibitors Enable >900 cm² Dynamic Windows based on Reversible Metal Electrodeposition with High Solar Modulation *Nat. Energy*, **2021**, *6*, 546-554.
- 6. Tao, X.; Liu, D.; Yu J.; Cheng, H. Reversible Metal Electrodeposition Devices: An Emerging Approach to Effective Light Modulation and Thermal Management. *Adv. Opt. Mater.*, **2021**, *9*, 2001847-2001856.
- 7. Granqvist, C. G. Electrochromic Oxides: A Unified View. *Solid State Ion.*, **1994**, 70-71, 678-685.
- 8. Lee E. S.; Yazdanian, M.; Selkowitz, S. E. *The Energy-Savings Potential of Electrochromic Windows in the US Commercial Buildings Sector*, **2004**.
- 9. Energy Savings Guide, https://view.com/sites/default/files/documents/product-guide.pdf, (accessed August 18, 2022).
- 10. U.S. Energy Information Administration, Consumption & Effiency, 2018, https://www.eia.gov/consumption/, accessed May 1, 2022.
- 11. Cai, G.; Wang, J.; Lee P. S. Next-generation Multifunctional Electrochromic Devices. *Acc. Chem. Res.*, **2016**, *49*, 1469-1476.
- 12. In, Y. R.; Kim, Y. M.; Lee Y.; Choi, W. Y.; Kim, S. H.; Lee, S. W.; Moon, H. C. Ultra-Low Power Electrochromic Heat Shutters Through Tailoring Diffusion-Controlled Behaviors. *ACS Appl. Mater. Inter.*, **2020**, *12*, 30635-30642.
- 13. Thakur, V. K.; Ding, G.; Ma, J.; Lee, P. S.; Lu, X. Hybrid Materials and Polymer Electrolytes for Electrochromic Device Applications. *Adv. Mater.*, **2012**, *24*, 4070-4070.
- 14. Granqvist, C. G. *Handbook of Inorganic Electrochromic Materials*, Elsevier Science, 1995.
- 15. Niklasson, G. A.; Granqvist, C. G. Electrochromics for Smart Windows: Thin Films of Tungsten Oxide and Nickel Oxide, and Devices based on These. *J. Mat. Chem.*, **2007**, *17*, 127-156.
- 16. Shi, P.; Amb, C. M.; Knott, E. P.; Thompson, E. J.; Liu D. Y.; Mei, J.; Dyer, A. L.; Reynolds, J. R. Broadly Absorbing Black to Transmissive Switching Electrochromic Polymers. *Adv. Mater.*, **2010**, *22*, 4949-4953.
- 17. Sanchez-Pena, J. M.; Vazquez, C.; Perez, I.; Rodriguez, I.; Oton, J. M. Electro-optic System for Online Light Transmission Control of Polymer-dispersed Liquid Crystal Windows *Opt. Eng.*, **2002**, *41*, 1608-1611.
- 18. Cupelli, D.; Nicoletta, F. P.; Manfredi, S.; Vivacqua, M.; Formoso, P.; De Filpo, G.; Chidichimo, G. Self-adjusting Smart Windows based on Polymer-dispersed Liquid Crystals. *Solar Energ. Mater. Solar C.*, **2009**, *93*, 2008-2012.
- 19. Coates, D. Polymer-dispersed Liquid Crystals J. Mat. Chem., 1995, 5, 2063-2072.
- 20. Kunwar, N.; Cetin, K. S.; Passe, U.; Zhou X.; Li, Y. Energy Savings and Daylighting Evaluation of Dynamic Venetian Blinds and Lighting through Full-scale Experimental Testing. *Energy*, **2020**, *197*, 117190-117202.
- 21. Galasiu, A. D.; Atif, M. R.; MacDonald, R. A. Impact of Window Blinds on Daylight-linked Dimming and Automatic On/off Lighting Controls. *Sol. Energy*, **2004**, *76*, 523-544.
- 22. Mortimer, R. J.; Dyer, A. L.; Reynolds, J. R. Electrochromic Organic and Polymeric Materials for Display Applications. *Displays*, **2006**, *27*, 2-18.

- 23. Garcia, G.; Buonsanti, R.; Llordes, A.; Runnerstrom, E. L.; Bergerud, A.; Milliron, D. J. Near-infrared Spectrally Selective Plasmonic Electrochromic Thin Films. *Adv. Opt. Mater.*, **2013**, *1*, 215-220.
- 24. Doane, J. W.; Golemme, A.; West, J. L.; Whitehead, J. B.; Wu, B. G. *Molecular Crystals and Liquid Crystals Incorporating Nonlinear Optics*, 1988, **165**, 511-532.
- 25. Aburas, M.; Ebendorff-Heidepriem, H.; Lei, L.; Li, M.; Zhao, J.; Williamson, T.; Wu Y.; Soebarto, V. Smart Windows–Transmittance Tuned Thermochromic Coatings for Dynamic Control of Building Performance *Energy Build.*, **2021**, *235*, 110717-110732.
- 26. How Much do Motorized Window Shades Cost?, https://omwavehome.com/featured/how-much-do-motorized-window-shades-cost/(accessed June 5, 2022).
- 27. Skywing, https://www.smartwingshome.com/ (accessed June 5, 2022).
- 28. Ziegler, J. P.; Howard, B. M. Applications of Reversible Electrodeposition Electrochromic Devices. *Solar Energ. Mater. Solar C.*, **1995**, *39*, 317-331.
- 29. Mascaro, L. H.; Kaibara, E. K.; Bulhões, L. O. An Electrochromic System based on the Reversible Electrodeposition of Lead. *J. Electrochem. Soc.*, **1997**, *144*, L273-L274.
- 30. Avellaneda C. O.; Napolitano, M. A.; Kaibara, E. K.; Bulhões, L. O. *Electrochim. Acta*, **2005**, *50*, 1317-1321.
- 31. Barile, C. J. Electrolyte Dynamics in Reversible Metal Electrodeposition for Dynamic Windows. *J. Appl. Electrochem.*, **2018**, *4*, 443-449.
- 32. DeFoor, C. L.; Jeanetta, J. F.; Barile, C. J. Controlling the Optical Properties of Dynamic Windows based on Reversible Metal Electrodeposition. *ACS Appl. Electron. Mater.*, **2020**, *2*, 290-300.
- 33. Cho, S. M.; Kim, S.; Kim, T. Y.; Ah, C. S.; Song, J.; Cheon, S. H.; Kim, J. Y.; Ryu, H.; Kim, Y. H.; Hwang C. S.; Lee J. I., New Switchable Mirror Device with a Counter Electrode based on Reversible Electrodeposition. *Solar Energ. Mater. Solar C.*, **2018**, 179, 161-168.
- 34. Ziegler, J. P. Status of Reversible Electrodeposition Electrochromic Devices. *Solar Energ. Mater. Solar C.*, **1999**, *56*, 477-493.
- 35. Hernandez, T. S.; Barile, C. J.; Strand, M. T.; Dayrit, T. E.; Slotcavage D. J.; McGehee, M. D. Bistable Black Electrochromic Windows based on the Reversible Metal Electrodeposition of Bi and Cu. *ACS Energy Lett.*, **2018**, *3*, 104-111.
- 36. Hernandez, T. S.; Alshurafa, M.; Strand, M. T.; Yeang, A. L.; Danner, M. G.; Barile, C. J.; McGehee, M. D. Electrolyte for Improved Durability of Dynamic Windows based on Reversible Metal Electrodeposition. *Joule*, **2020**, *4*, 1501-1513.
- 37. Strand M. T.; Barile C. J.; Hernandez, T. S.; Dayrit, T. E.; Bertoluzzi L.; Slotcavage, D. J.; McGehee, M. D. Factors that Determine the Length Scale for Uniform Tinting in Dynamic Windows based on reversible metal electrodeposition. *ACS Energy Lett.*, **2018**, 3, 2823-2828.
- 38. O. S. New York: Dover Publications, *Optical Properties of Thin Solid Films* Dover Publications, Inc., New York, 1965.
- 39. Greenword, N. N.; Earnshaw, A. Chemistry of the Elements, Butterworth-Heinemann, Oxford, U.K., 2nd ed., 1997.
- 40. Tierney, M. J.; Martin, C. R. Transparent Metal Microstructures. *J. Phys. Chem.*, **1989**, 93, 2878-2880.

- 41. Johnson P.; Christy R. Optical Constants of Transition Metals: Ti, V, Cr, Mn, Fe, Co, Ni, and Pd. *Phys. Rev. B*, **1974**, *9*, 5056-5070.
- 42. Bao S.; Tajima, K.; Yamada, Y.; Okada M.; Yoshimura, K. Color-neutral Switchable Mirrors based on Magnesium-titanium Thin Films *Appl. Phys. A*, **2007**, *87*, 621-624.
- 43. Araki, S.; Nakamura, K.; Kobayashi, K.; Tsuboi A.; Kobayashi, N. Electrochemical Optical-modulation Device with Reversible Transformation between Transparent, Mirror, and Black *Adv. Mater.*, **2012**, *24*, Op122-Op126.
- 44. Tsuboi, A.; Nakamura K.; Kobayashi, N. A Localized Surface Plasmon Resonance-Based Multicolor Electrochromic Device with Electrochemically Size-Controlled Silver Nanoparticles. *Adv. Mater.*, **2013**, *25*, 3197-3201.
- 45. Park, C.; Seo, S.; Shin, H.; Sarwade, B. D.; Na, J.; Kim, E. Switchable Silver Mirrors with Long Memory Effects. *Chem. Sci.*, **2015**, *6*, 596-602.
- 46. Li, J. Y.; Juarez-Rolon, J. S.; Islam, S. M.; Barile, C. J. Electrolyte Effects in Reversible Metal Electrodeposition for Optically Switching Thin Films. *J. Electrochem. Soc.*, **2019**, *166*, D496-D504.
- 47. Madu, D. C.; Islam, S. M.; Pan, H.; Barile, C. J. Electrolytes for Reversible Zinc Electrodeposition for Dynamic Windows *J. Mater. Chem. C*, **2021**, *9*, 6297-6307.
- 48. Smith, K. S.; Huyck, H. L. *The Environmental Geochemistry of Mineral Deposits*, **1999**, 6, 29-70.
- 49. Winder, C.; *Toxicity of Metals*, CRC Press Boca Raton, 2004.
- 50. Chen, M. H. Resources Policy, **2010**, *35*, 127-140.
- 51. Popp, J.; Oláh, J.; Farkas Fekete, M.; Lakner, Z.; Máté, D. From Basic Research to Competitiveness: An Econometric Analysis of the Global Pharmaceutical Sector. *Energies*, **2018**, *11*, 2392-2410.
- 52. Vanýsek, P. *CRC Handbook of Chemistry and Physics*, CRC Press, Boca Raton, Florida, 2002.
- 53. Miller, D. D.; Li, J. Y.; Islam, S. M.; Jeanetta, J. F.; Barile, C. J. *J. Mat. Chem. C*, **2020**, 8, 1826-1834.
- 54. Li, J. Y.; Barile, C. J. Reversible Electrodeposition of Ni and Cu for Dynamic Windows. *J. Electrochem. Soc*, **2021**, *168*, 092501-092508.
- 55. Kim, H. I.; Kim, E. J.; Kim, S. J.; Shin, H. C. Influence of ZnO Precipitation on the Cycling Stability of Rechargeable Zn–air Batteries. *J. Appl. Electrochem.*, **2015**, *45*, 335-342.
- 56. Yuan, L.; Hao, J.; Kao, C.; Wu, C.; Liu, H.; Dou, S.; Qiao, S. Regulation Methods for the Zn/electrolyte Interphase and the Effectiveness Evaluation in Aqueous Zn-ion Batteries. *Energ. Env. Sci.* **2021**, *14*, 5669-5689.
- 57. Quaino, P.; Juarez, F.; Santos, E.; Schmickler, W. Volcano Plots in Hydrogen Electrocatalysis–Uses and Abuses. *Beilstein Journal of Nanotechnology*, **2014**, *5*, 846-854
- 58. Musei, N. N.; Onu, C. E.; Ihuaku, K. I.; Igbokwe, P. K. Effects of Lithium Sulfate and Zinc Sulfate Additives on the Cycle Life and Efficiency of Lead Acid Batteries. *ACS Omega*, **2021**, *6*, 4423-4429.
- 59. Wang, N.; Wan, H.; Duan, J.; Wang, X.; Tao L.; Zhang, J.; Wang, H. A Review of Zinc-based Battery from Alkaline to Acid. *Mater. Today Adv.*, **2021**, *11*, 100149-100168.
- 60. Karimi M. A.; Karami, H.; Mahdipour, M. Sodium Sulfate as an Efficient Additive of Negative Paste for Lead-acid Batteries. *J. Power Sources*, **2006**, *160*, 1414-1419.

- 61. Yeang, A. L.; Hernandez, T. S.; Strand, M. T.; Slotcavage, D. J.; Abraham, E.; Smalyukh, I. I.; Barile, C. J.; McGehee, M. D. Transparent, High-Charge Capacity Metal Mesh Electrode for Reversible Metal Electrodeposition Dynamic Windows with Dark-State Transmission <0.1%. *Adv. Energ. Mater.*, **2022**, *12*, 2200854-2200864.
- 62. Islam, S. M.; Barile, C. J. Dynamic Windows using Reversible Zinc Electrodeposition in Neutral Electrolytes with High Opacity and Excellent Resting Stability. *Adv. Energ. Mater.*, **2021**, *11*, 2100417-2100424.
- 63. Vieira, N. C. S.; Fernandes, E. G. R.; de Queiroz, A. A. A.; Guimaraes, F. E. G.; Zucolotto, V. Indium Tin Oxide Synthesized by a Low Cost Route as SEGFET pH Sensor. *Mater. Res.*, **2013**, *16*, 1156-1160.
- 64. Moezzi, A.; Cortie, M. B.; McDonagh, A. M. Zinc Hydroxide Sulphate and its Transformation to Crystalline Zinc Oxide. *Dalton Trans.*, **2013**, *42*, 14432-14437.
- 65. Liang, W.; Li, W.; Chen, H.; Liu, H.; Zhu, L. Exploiting Electrodeposited Flower-like Zn₄(OH)₆SO₄-4H₂O Nanosheets as Precursor for Porous ZnO Nanosheets. *Electrochim. Acta*, **2015**, *156*, 171-178.
- 66. Hosseini, S.; M. Soltani, S.; Li, Y. Y. Current Status and Technical Challenges of Electrolytes in Zinc–air Batteries: An In-depth Review. *Chem. Eng. Journal*, **2021**, *408*, 127241-127262.
- 67. Wang, M.; Jiang, L.; Kim, E. J.; Hahn, S. H. Electronic Structure and Optical Properties of Zn(OH)₂: LDA+U Calculations and Intense Yellow Luminescence. *RSC Adv.*, **2015**, *5*, 87496-87503.
- 68. Sun, K. E. K.; Hoang, T. K. A.; Doan, T. N. L.; Yu, Y.; Zhu, X.; Tian, Y.; Chen, P. Supression of Dendrite Formation and Corrosion on Zinc Anode of Secondary Aqueous Batteries. *ACS Appl. Mater. Inter.*, **2017**, *9*, 9681-9687.
- 69. Mandal, S; Samanta, P. K. Electrochemical Growth of Metallic Zinc and its Crystallographic Study using Rietveld. *Mater. Today*, **2021**, *43*, 3091-3094.
- 70. Ullah, S.; Badshah, A.; Ahmed, F.; Raza, R.; Altaf, A.; Hussain, R. Electrodeposited Zinc Electrodes for High Current Zn/AgO Bipolar Batteries. *Int. J. Electrochem. Sci.*, **2011**, *6*, 3801-3811.

